The 15th International Symposium on Magnetic Bearings, August 3-6, 2016, Mojiko Hotel, Kitakyushu, Japan

ISMB15

Evaluation of the electrodynamic forces in high-speed permanent magnet machines with rotor eccentricity

Corentin DUMONT*, Adrien GILSON**, Virginie KLUYSKENS*, Christophe ESPANET** and Bruno DEHEZ*

* Center for Research in Mechatronics, Université catholique de Louvain
Place du Levant 2, Louvain-la-Neuve 1348, Belgium
E-mail: corentin.dumont@uclouvain.be

** Energy Department, FEMTO-ST Institute, University of Franche-Comté
Avenue Jean Moulin 2, Belfort 90000, France

Abstract

In permanent magnet motors, the presence of rotor eccentricities can alter the airgap field distribution. This results in parasitic radial detent forces that can be reduced by connecting the stator phases in parallel. As a consequence, currents are passively induced in the windings when the rotor spins in an off-centered position, yielding balancing electrodynamic forces. Specific models were developed to predict these forces, but their complexity can be prohibitive. Therefore, this paper proposes to study the effect of the rotor off-centering in permanent magnet motors using a simpler model developed for electrodynamic bearings. This model consists in a linear differential equation with only four parameters that depend neither on the spin speed nor on the rotor position. As an illustration, the paper applies this model to the study of a high-speed, slotted permanent magnet motor. To support this, the main hypotheses of the model are validated in this particular case. Finally, the centering electrodynamic forces in a quasi-static configuration are predicted using the model and compared to finite element simulation results.

Key words : Synchronous, Motor, Eccentricity, Force, Passive, Electrodynamic, Model

1. Introduction

Bearing wear and manufacturing tolerances can lead to rotor eccentricities in permanent magnet (PM) machines. This affects the symmetry of the field distribution in the airgap, thereby creating a radial detent force known as unbalanced magnetic pull (UMP) (Rahideh and Korakianitis, 2011) (Dorrell et al., 2009). The UMP is a potential source of excessive noise, vibrations, and additional wear of the mechanical bearings (Kim and Lieu, 2005) (Li et al., 2011). Therefore, passive and active strategies have been studied to reduce these effects. Among them, the parallel connection of the stator windings is well known (Burakov and Arkkio, 2007) (Kasten and Redemann, 2014). It allows passively induced currents to flow in the stator windings when the rotor spins in an off-centered position, thereby creating forces that balance the UMP.

Different models predicting the balancing forces in permanent magnet (PM) motors have been proposed (Burakov and Arkkio, 2006) (Dorrell and Ionel, 2012). These models can be adapted to a wide range of machines. However, they include assumptions on the rotor motion so that only static and dynamic eccentricities are considered, and the model parameters must be re-estimated if the operating point of the motor changes.

The operation of heteropolar electrodynamic bearings (EDBs) is also based on passively induced centering forces. In particular, the origin of these forces is the same as in PM motors with parallel winding connections. When the rotor is off-centered, the PM field distribution changes in the air gap, thereby creating additional harmonics that increase with the off-centering (Rahideh and Korakianitis, 2011). If the main harmonics in the initial PM field distribution has one pair of poles, the most significant harmonic created by the off-centering has two pole pairs. On the one hand, these harmonics have a negative effect since their interaction yields the UMP (Chiba et al., 2005). On the other hand, the two pole pairs harmonic can be linked by a winding that also has two pole pairs, thereby inducing balancing currents which tend to restore the centered position of the rotor (Dumont et al., 2014). Similarly, in the case of a one pole pair PM motor, the

parallel connection of each motor phase may allow for the existence of conducting paths with two pole pairs and passive centering forces.

Recent advances in the modeling of EDBs lead to the derivation of a linear equation predicting the dynamics of the bearing rotor (Dumont et al., 2016). This model includes no assumption on the rotor motion and spin speed. It depends on only four parameters that are identified through a limited number of quasi-static simulations.

In this context, this paper first proposes a method for predicting the passive electrodynamic forces in brushless PM motors using the model developed for heteropolar EDBs (Dumont et al., 2016). This model is then applied in the practical case of a high-speed DC motor dedicated to air compression that is currently being designed at the FEMTO-ST institute (Gilson et at., 2015). For example, the model could be used to investigate the presence of radial forces due to the use of air bearings that allows for small radial displacements of the rotor.

The paper is organized as follows. In section 2, the motor topology and winding connections are introduced. In section 3, the EDB model is presented and applied to the motor case. In section 4, the main hypotheses of the model are validated and the parameters corresponding to the study case are identified. Finally, the model is exploited to predict the radial forces on the off-centered rotor in section 5.

2. Motor and phases connection

Figure 1a shows the topology of the motor used as an example in this paper. The motor is designed for high-speed applications such as air compression. Therefore, it has a large airgap and a retaining sleeve around the PMs. The parameters of the motors are given in Tables 1 and 2. The nominal airgap is denoted $g = R_s - R_{sl}$.

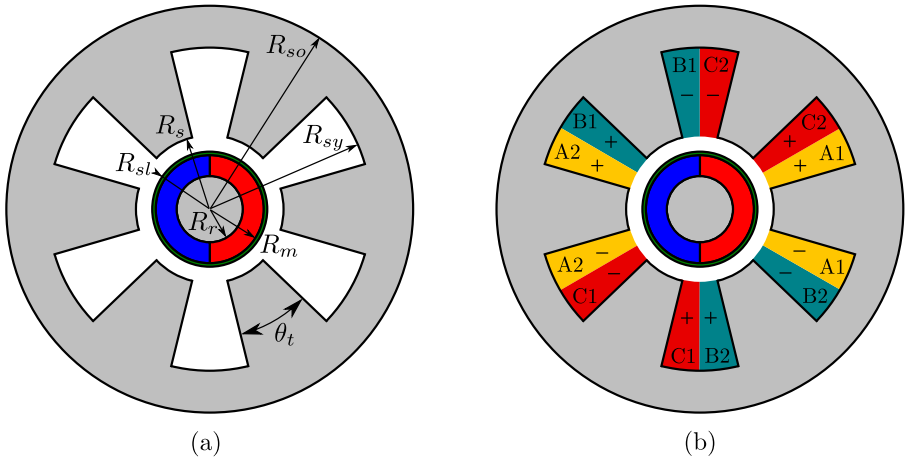

Fig. 1 Motor topology and phases arrangement. (a) Geometrical parameters of the motor. The internal rotor comprises surface-mounted PMs with one pole pair and a retaining sleeve. (b) The winding has three phases composed of two concentrated coils. For example, the coils A1 and A2 constitute phase A.

Table 1 Motor geometrical parameters.

Parameters	Values
R_{so}	35 mm
R_{sy}	27.8 mm
R_s	12.7 mm
R_{sl}	9.9 mm
R_m	9.3 mm
R_r	5.7 mm
θ_t	32.4°
Axial length L	30 mm

Table 2 Other motor parameters.

Parameters	Values
Remanent field density of the PM	1.2 T
Copper conductivity σ_c	$6e7$ S/m
Slot fill factor r	0.5
Relative permeability of the PMs, retaining sleeve, and winding	1
Relative permeability of the rotor shaft and stator yoke	∞
Number of wire turns around each slot N	10

The stator yoke has six slots and three phases, each of them being composed of two concentrated winding coils. As shown in Fig. 2, the coils can be connected in series or in parallel. In this paper, only the parallel connection is considered

as it allows for passively induced currents to flow in the winding paths shown by the arrows in Fig. 2a. These paths have two pole pairs and are referred to as the suspension phases in the next sections. Let us note that there can be a non zero motor phase current with a zero suspension phase current and vice-versa.

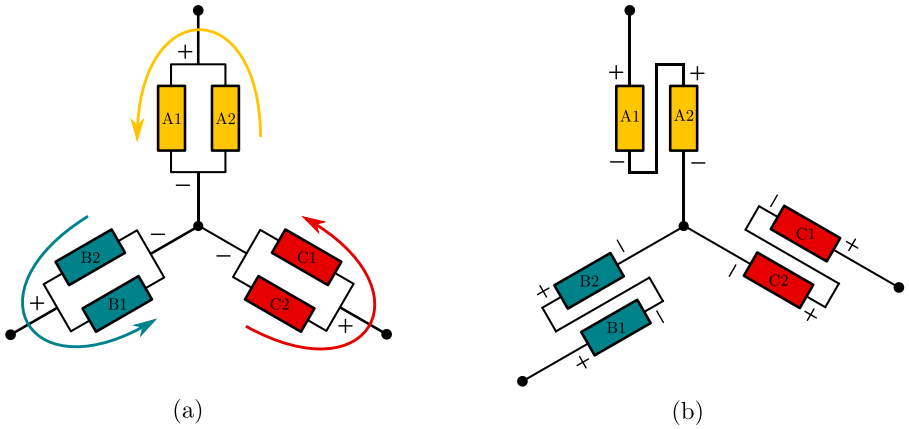

Fig. 2 Two different motor phase coils connections. (a) Phase coils connected in parallel. The arrows show the short-circuited current paths for the suspension currents. (b) Phase coils connected in series. There are no possible current paths in the windings for the suspension currents.

3. Modeling

Initially, this motor was designed for high-speed applications without considering a rotor off-centering. However, in case of rotor off-centering, passively induced currents flow in the motor phases that are connected in parallel, resulting in balancing forces. These passive electrodynamic forces can be predicted using the model initially developed for EDBs (Dumont et al., 2016). This model links the radial forces to the rotor position through a linear equation with constant coefficients:

$$\dot{F} = -\frac{R}{L_c}F - j\omega F - K_d\dot{z} - \frac{3K_\Phi^2}{2L_c}\dot{z} - \frac{RK_d}{L_c}z - j\omega z K_d - j\omega z\frac{3K_\Phi^2}{2L_c}, \tag{1}$$

where the forces and rotor displacements are expressed in the stator frame using the complex notations $F = F_x + jF_y$ and $z = x + jy = |z|e^{j\phi}$, respectively. The parameters R is the phase resistance of a suspension phase, K_d is the negative stiffness associated with the detent force between the PMs and the stator yoke, and K_Φ is the PM flux constant defined in hypothesis 8 below. The cyclic inductance is $L_c = L - M$, where L and M are the self- and mutual inductances of the suspension phases, respectively.

The model was derived under the following assumptions:

(1) the rotor spin speed ω is an input of the system and is constant;
(2) only translational eccentricity is considered, i.e., the magnetic axis of the rotor and winding remain parallel;
(3) the materials have linear magnetic characteristics and therefore magnetic hysteresis and saturation are neglected;
(4) there is no proximity or skin effect in the conductors;
(5) the eddy currents are neglected in the PMs, in the sleeve and in the stator yoke;
(6) the impact of the rotor off-centering $|z|$ on the winding inductances is neglected;
(7) the detent force F_d between the PMs and the yoke obeys: $F_d = -K_d z$, where the detent stiffness K_d is real and negative;
(8) the PM flux linked by a suspension phase Φ_{Mk} obeys: $\Phi_{Mk} = |z|K_\Phi \cos\left(\omega t + \phi + \frac{2\pi(k-1)}{3}\right)$, where $k \in \{1, 2, 3\}$ is the phase number;
(9) the motor currents do not impact the radial forces on the rotor.

Finally, let us note that the coefficients K_d, K_Φ^2/L_c, and R/L_c in Eq. (1) do not depend on the number of winding turns N. Therefore, N has no impact on the forces and can be chosen considering only the constraints associated with the motor function.

4. Parameters identification and hypotheses validation

In this section, the parameters from Eq. (1) are evaluated, and the hypotheses 6-9 of the model are validated using two-dimensional quasi-static finite element (FE) simulations. The magnetic permeability of the shaft and yoke was set to $\mu_r = 1000$ in the FE model.

4.1. Suspension phase resistance

The suspension phase resistance is obtained without taking the end-windings into account. Considering the motor parameters from Table 1 and 2, this yields:

$$R = \frac{48LN^2}{\sigma_c r\pi \left(R_{sy}^2 - R_s^2\right)\left(1 - \frac{\theta_t}{60}\right)} = 5.4[m\Omega]. \tag{2}$$

4.2. Radial detent force

Let us study the radial forces in the absence of currents in the suspension phases. When the rotor is off-centered, the symmetry of the magnetic field in the airgap is broken. This results in a parasitic attraction force between the rotor and the stator. This force has two components acting in the direction of the off-centering z and in the direction perpendicular to it. Assuming that they are proportional to the off-centering, they can be associated with the stiffnesses:

$$K_{d,\parallel} = -\Re\left\{\frac{F}{z}\right\} \tag{3}$$

$$K_{d,\perp} = -\Im\left\{\frac{F}{z}\right\}. \tag{4}$$

From the model assumptions in section 3, $K_{d,\perp}$ is neglected and the value of $K_{d,\parallel}$ is constant and does not depend on the rotor position. Furthermore, it is assumed that the forces on the rotor in the absence of suspension currents are detent forces only i.e., the impact of the currents flowing in the motor phases is neglected.

Let us validate this by calculating $K_{d,\perp}$ and $K_{d,\parallel}$ for two different kinds of rotor motion. Figure 3a corresponds to the static eccentricity configuration, i.e. the rotor spins in a fixed position $z = g/2$. Figure 3b corresponds to the dynamic eccentricity configuration, i.e. the rotor center whirls around the stator center so that $|z| = g/2$, while $\omega = 0$. In the absence of motor currents, the mean value of $K_{d,\parallel}$ is $K_d = -16.96[kN/m]$, whereas the amplitude of $K_{d,\perp}$ does not exceed 4% of K_d for both kinds of rotor motion.

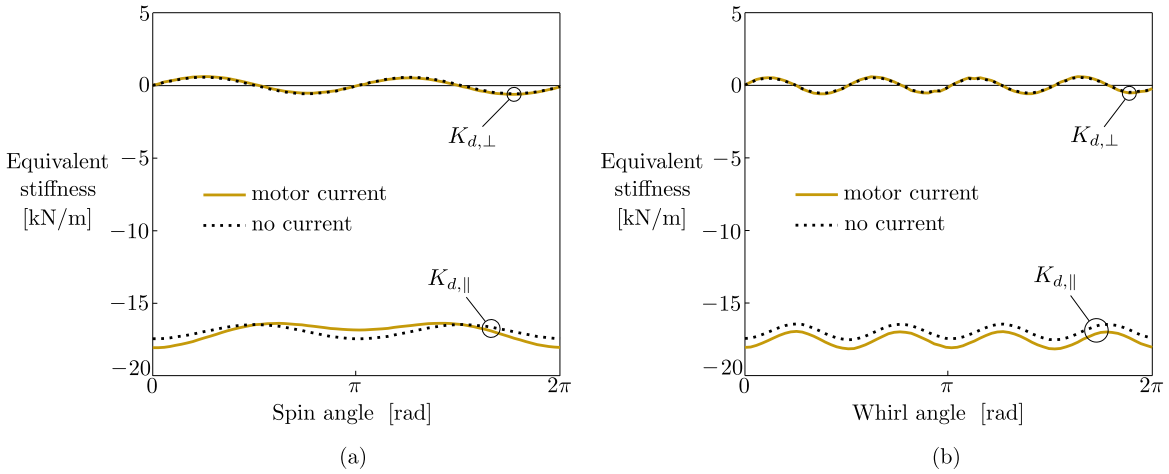

Fig. 3 Amplitude of the equivalent stiffness between the rotor and the stator in the absence of suspension currents. The motor currents are set to zero or to maximum values so that $I_A = -2I_B = -2I_C$, where I_A is such that the current density on the copper cross-section of phase A reaches $5[A/mm^2]$. (a) Data obtained in a static eccentricity configuration. (b) Data obtained in a dynamic eccentricity configuration.

The impact of the motor currents is obtained by setting $I_A = -2I_B = -2I_C$, where I_A is such that the current density on the copper cross-section of phase A reaches the maximum value of $5[A/mm^2]$. In presence of motor currents, the value

of $K_{d,\parallel}$ does not differ by more than 7% of the value of $K_d = -16.96[kN/m]$, whereas the amplitude of $K_{d,\perp}$ does not exceed 4% of K_d for both kinds of rotor motion. Finally, other simulations were carried out under the same conditions but with different eccentricities in the range $[0, g/2]$. They showed that the impact of the eccentricity on K_d is small too.

In the next sections, the impact of the off-centering and motor currents on $K_{d,\perp}$ is neglected and $K_{d,\parallel}$ is assumed to be constant: $K_{d,\parallel} \approx K_d = -16.96[kN/m]$, and $K_{d,\perp} \approx 0[kN/m]$.

4.3. PM flux linked by the suspension and motor phases

Let us validate hypothesis 8, which states that only the main PM flux harmonic is considered in the suspension phases, and that it is proportional to the off-centering $|z|$. In this aim, the value of $K_\Phi = 0.486[Wb/m]$ is identified by evaluating the amplitude of the main PM flux harmonic in the suspension phase A when the rotor spins at $z = g/4$. This corresponds to the 'fitting curve' in Fig. 4a. As shown in Fig. 4, the PM flux in each suspension phase can then be predicted through the PM flux equation in hypothesis 8. These predictions are then compared to FE results for different amplitudes of the eccentricity ($g/4$ and $g/2$), and for two different kinds of motion.

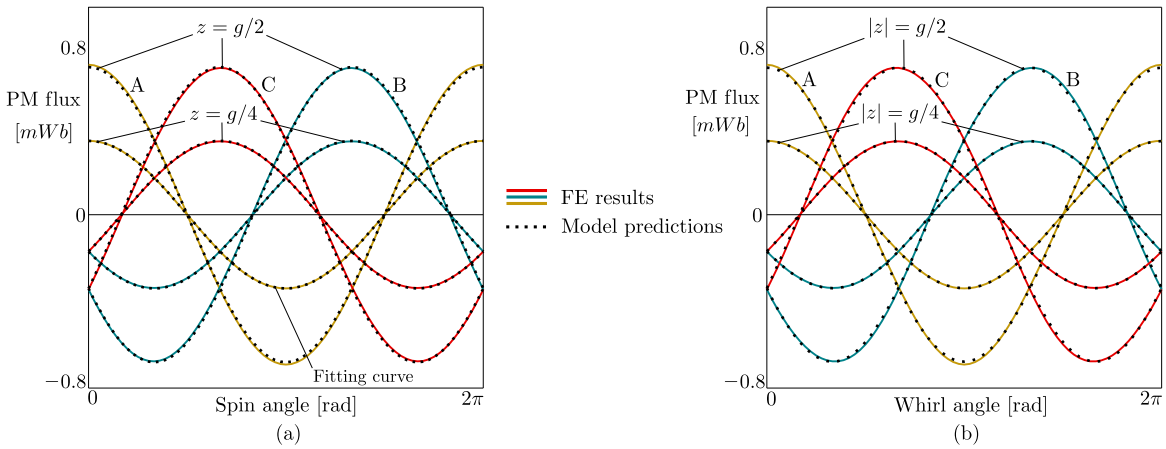

Fig. 4 Comparison between FE and the model predictions of the PM flux in the suspension phases. The rotor eccentricity is set to $g/4$ and $g/2$. Coefficient K_Φ is identified using the data of the 'fitting curve', allowing to predict the PM flux in each winding phase when the rotor (a) spins or (b) whirls, for example.

In conclusion, the previous results validate assumption 8 for the PM flux in the suspension phases as the evolution of the PM flux assumed by the model is close to the FE results.

4.4. Winding inductances

Due to the presence of a ferromagnetic shaft, a rotor off-centering impacts the mutual inductances of the suspension windings. Assuming a whirling rotor motion with $|z| = g/2$, Fig. 5 shows the ratio of the mutual inductances between the suspension phases to their respective average values. The impact of the off-centering on the mutual inductances does not exceed 0.5% of their average value and is thus neglected.

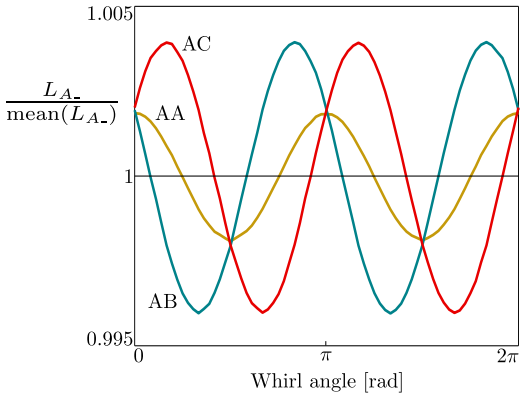

Fig. 5 Ratio of the mutual inductances between the suspension phases to their respective average values.

In conclusion, assumption 6 regarding the inductances is confirmed. From the FE results, the cyclic inductance of

the suspension windings is obtained by combining the mutual inductances obtained when the rotor is centered. Assuming a single winding turn, this yields:

$$L_c = L_{AA} - \frac{1}{2}L_{AB} - \frac{1}{2}L_{AC} = 32.5[\mu H]. \tag{5}$$

5. Forces prediction

The accuracy of the model force predictions are validated through a comparison with FE simulation results. In this aim, a transient FE model of the motor is run using the following approach. The motor is fed with three-phase balanced sinusoidal currents so that the peak current density in each phase is $5[A/mm^2]$. The radial forces are then obtained in a static eccentricity configuration for different spin speeds and eccentricities. Figure 6a and b show the average values of $F_\parallel$ and $F_\perp$ calculated over one full revolution of the rotor. They are denoted $\bar{F}_\parallel$ and $\bar{F}_\perp$, respectively. As the model is transient, it was run during more than $5\tau = 5L_c/R[s]$ before recording the data in order to ensure that the suspension currents have reached a steady state.

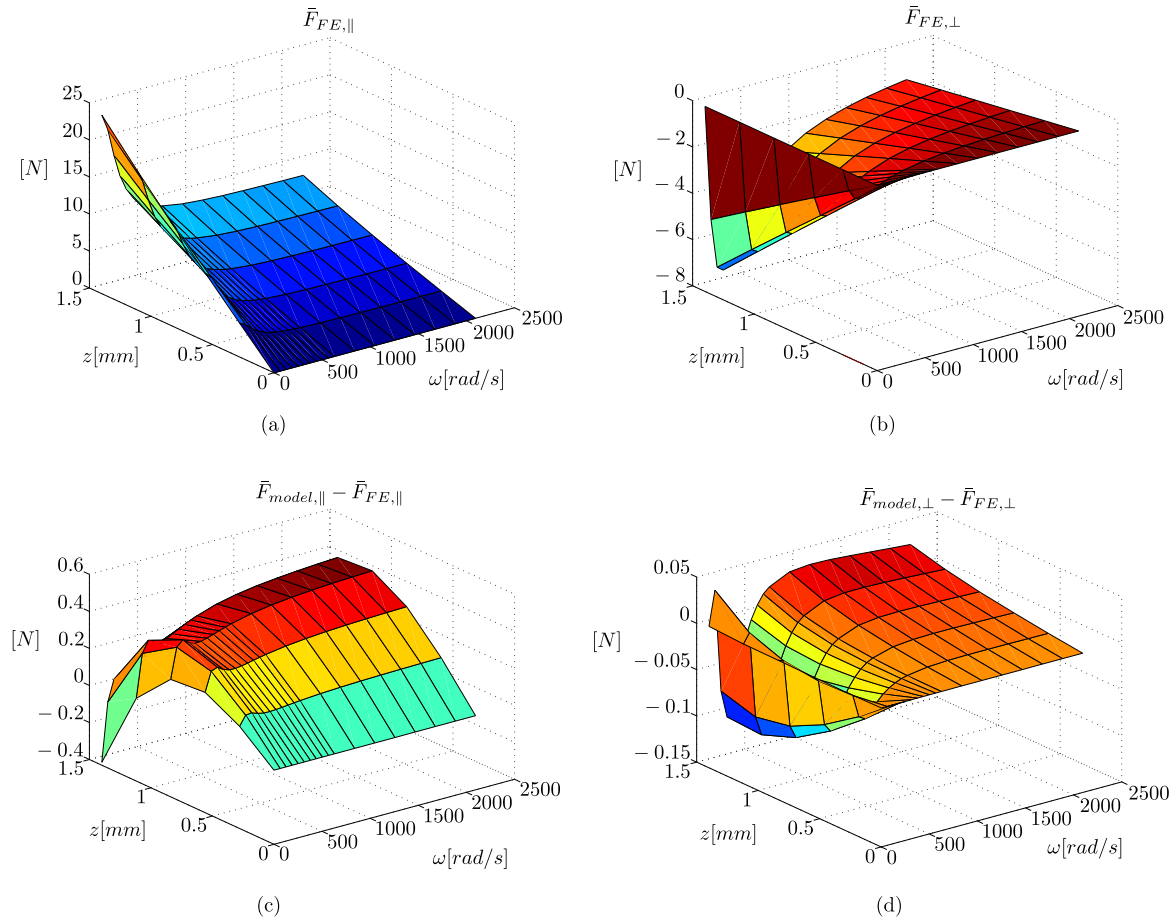

Fig. 6 Forces on the rotor spinning in a static eccentricity configuration. (a) and (b) Average forces $\bar{F}_\parallel$ and $\bar{F}_\perp$ from FE results. (c) and (d) Difference between the FE results and the model predictions of the average forces $\bar{F}_\parallel$ and $\bar{F}_\perp$.

Let us analyze these results. At zero spin speed, there is no electrodynamic centering force. Only the detent force acts in the direction of the off-centering and its amplitude is given by the curve $\omega = 0[rad/s]$ in Fig. 6a. At higher values of ω, the centering electrodynamic force increases and saturates above $\omega = 600[rad/s]$. This effect is significant, resulting in a reduction of $\bar{F}_\parallel$ to 40% of its value at zero spin speed. Despite this reduction, the electrodynamic force is not sufficient to fully counterbalance the detent force. On the other hand, $\bar{F}_\perp$ can also reach significant values of up to $-7.2[N]$ at $z = 1.4[mm]$ and $\omega = 189[rad/s]$. This value decreases at higher speeds.

Finally, the model predictions and FE results are compared in Fig. 6c and d, showing the accuracy of the model to predict the centering forces.

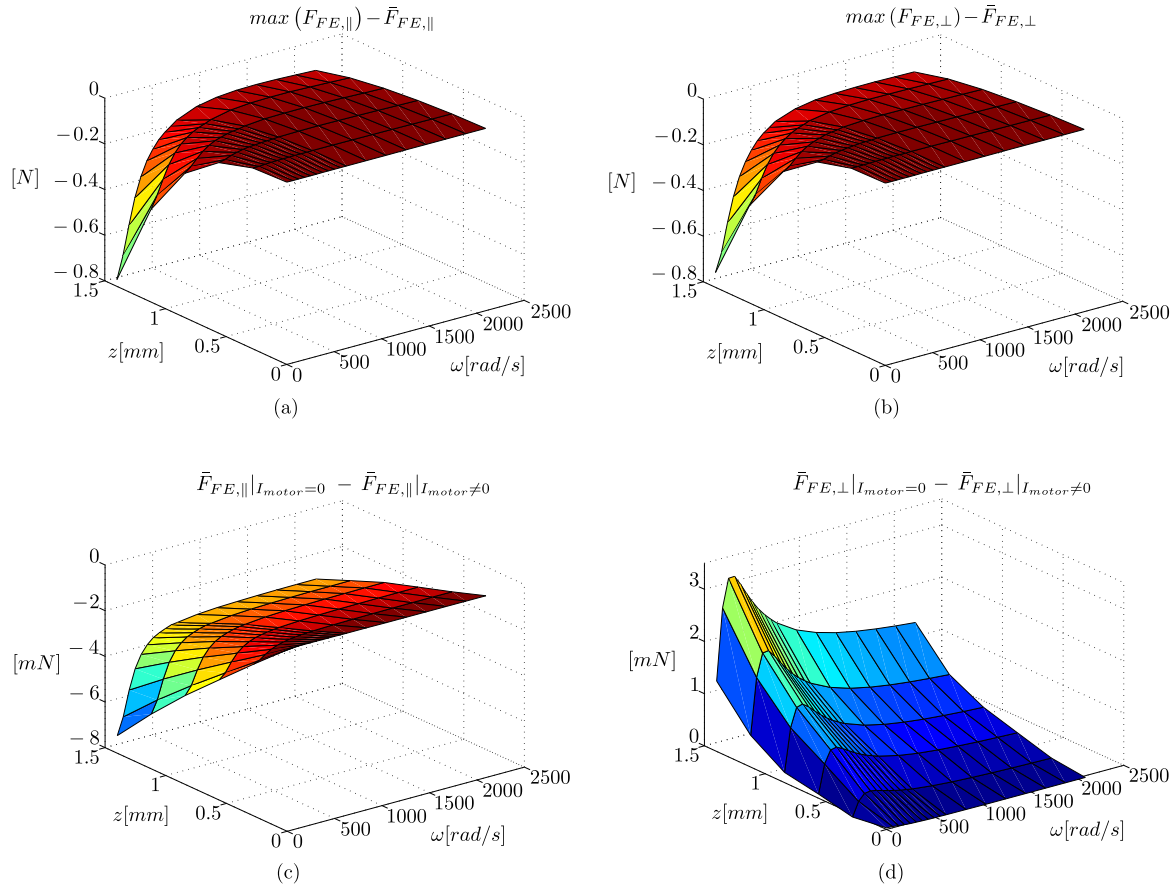

Fig. 7 Forces on the rotor spinning in a static eccentricity configuration. (a) and (b) Maximum difference between FE predictions of $F_\parallel$ and $F_\perp$ and their respective average values. (c) and (d) Difference between the average forces on the rotor, with and without motor currents.

The model predicts that the amplitude of the forces is constant in the static eccentricity configuration. Its predictions fit well to the average values of the forces obtained from the FE simulations, as shown in Fig. 6 (c) and (d). However, the amplitude of the forces can vary with the angular position of the rotor, according to the FE results. Let us now compare the maximum values of $F_\parallel$ and $F_\perp$ to their respective average values. As shown in Fig. 7 (a) and (b), the absolute difference between the maximum and average values of the forces is moderate. In relative terms and for $F_\parallel$, this difference does not exceed 3% of its average value within the domain shown in Fig. 7 (a). For $F_\perp$, the relative difference remains also low except at low speed and for large eccentricities, where the relative error peaks up because the force amplitude approaches zero.

Lastly, the average forces $\bar{F}_\parallel$ and $\bar{F}_\perp$ are calculated in the absence of motor currents. The difference between the average forces with and without the motor currents are negligible, as shown in Fig. 7(c) and (d). This validates assumption 9 from section 3.

6. Conclusion

This paper detailed how the most important assumptions of the EDB model can be validated to show its applicability in the case of a motor with parallel connections in the stator windings. These assumptions are verified for the slotted PM motor that is being designed at the FEMTO-ST institute. In this case, it was shown that the suspension function can be studied separately from the motor function. As a validation of the model, the force predictions were compared with FE simulation results, showing a good agreement between them. In particular, the model shows a good accuracy at low eccentricities, which corresponds to the most likely operating conditions of the motor.

Finally, this study showed that the electrodynamic force cannot fully compensate the detent force in the present motor. However, the effect of the detent force can be reduced by up to 60% of its value in the absence of electrodynamic forces.

From a theoretical point of view, further studies could include a more detailed analysis of the coupling between the suspension and motor functions. Also, other kinds of rotor eccentricities should also be simulated to better illustrate the potential of the model when it comes to predicting the forces for various kinds of rotor motion. From a design point of view, the impact of the off-centering on the copper losses should be quantified. The possibility of further reducing the UMP through the use of non-ferromagnetic materials for the slots could also be investigated.

References

Burakov, A. and Arkkio, A., Low-order parametric force model for eccentric-rotor electrical machine with parallel connections in stator winding, IET Electric Power Applications, Vol.1, No.4, (2006), pp.592-600.

Burakov, A. and Arkkio, A., Comparison of the unbalanced magnetic pull mitigation by the parallel paths in the stator and rotor windings, IEEE Transactions on Magnetics, Vol.43, No.12 (2007), pp.4083-4088.

Chiba, A., Fukao, T., Ichikawa, O., Takemoto, M., Dorrell, D. G., Magnetic Bearings and Bearingless Drives (2005), pp. 313-315, Newnes.

Dorrell, D. G., Hsieh, M. F., Guo, Y., Unbalanced magnet pull in large brushless rare-earth permanent magnet motors with rotor eccentricity, IEEE Transactions on Magnetics, Vol.45, No.10 (2009), pp.4586-4589.

Dorrell, D. G., Ionel, D., Radial forces and vibrations in permanent magnet and induction machines, Proceedings of the IEEE Power and Energy Society General Meeting (2012), pp. 1-6.

Dumont, C., Kluyskens, V., Dehez, B., Null flux radial electrodynamic bearing, IEEE Transactions on Magnetics, Vol.50, No.10 (2014), pp.1-12.

Dumont, C., Kluyskens, V., Dehez, B., Linear state-space representation of heteropolar electrodynamic bearings with radial magnetic field, IEEE Transactions on Magnetics, Vol.52, No.1 (2016), pp.1-9.

Gilson, A., Tavernier, S., Gerber, M., Espanet, C., Dubas, F., Depernet, D., Design of a cost-efficient high-speed high-efficiency PM machine for compressor applications, 2015 IEEE Energy Conversion Congress and Exposition (ECCE) (2015), pp. 38523856.

Kasten, H. and Redemann, C., Influence on unbalanced magnetic pull, Proceedings of the 14th International Symposium on Magnetic Bearings (ISMB14) (2014), pp.758-761.

Kim, U. and Lieu, D. K., Effects of magnetically induced vibration force in brushless permanent-magnet motors, IEEE Transactions on Magnetics, Vol.41, No.6 (2005), pp.2164-2172.

Li, J. T., Liu Z. J. and Nay, L. H. A, Effect of radial magnetic forces in permanent magnet motors with rotor eccentricity, IEEE Transactions on Magnetics, Vol. 43, No.6 (2007), pp.2525-2527.

Rahideh, A., Korakianitis, T., Analytical open-circuit magnetic field distribution of slotless brushless permanent-magnet machines with rotor eccentricity, IEEE Transactions on Magnetics, Vol. 47, No.12 (2011), pp.4791-4808.